

Cite this: DOI: 00.0000/xxxxxxxxxx

A versatile deep learning-based protein–ligand interaction prediction model for accurate binding affinity scoring and virtual screening[†]

Seokhyun Moon,^a Sang-Yeon Hwang,^b Jaechang Lim,^b and Woo Youn Kim^{*abc}

Received Date

Accepted Date

DOI: 00.0000/xxxxxxxxxx

Protein–ligand interaction (PLI) prediction is critical in drug discovery, aiding the identification and enhancement of molecules that effectively bind to target proteins. Despite recent advances in deep learning-based PLI prediction, developing a versatile model capable of accurate binding affinity scoring and virtual screening in PLI prediction is an ongoing challenge. This is primarily due to the lack of structure–affinity data, resulting in low model generalization ability. We here propose a viable solution to this challenge by introducing a novel data augmentation strategy along with a physics-informed neural network. The resulting model exhibits significant improvement in both scoring and screening capabilities. Its performance was compared to task-specific deep learning-based PLI prediction models, confirming its versatility. Notably, it even outperformed computationally expensive molecular dynamics simulations as well as the other deep learning models in a derivative benchmark while maintaining sufficiently high performance in virtual screening. This underscores the potential of this approach in drug discovery, demonstrating its applicability to both binding affinity scoring and virtual screening.

1 Introduction

Predicting protein–ligand interaction (PLI) plays a critical role in the early stages of drug discovery, facilitating the discovery and improvement of molecules that effectively bind to target proteins.^{1–3} It can be mainly utilized for two purposes: a process designed to refine these discovered molecules to increase their affinity for the target protein and virtual screening to efficiently identify hit candidates from a large chemical space. The binding affinity improvement process places greater emphasis on accuracy due to the need for precise evaluation of a relatively smaller number of molecules,^{4,5} while virtual screening emphasizes cost-effectiveness due to the extensive calculation required.^{6,7} In this light, both fast and accurate PLI prediction is necessary to meet these requirements. An ideal PLI prediction model should be computationally efficient and accurate in predicting binding affinity and thus be able to correlate the prediction with experimental binding affinities or correctly distinguish active molecules and decoy molecules.^{8,9}

Recently, deep learning-based models have emerged as a new avenue for PLI prediction.^{10–13} Deep learning allowed for retaining fast computation speed while demonstrating better performance in predicting binding affinity for protein–ligand crystal structures.¹⁴ Despite their potential, most deep learning-based PLI prediction models are insufficient to be applied to various tasks at once.^{15–18} Instead, they are task-specific, focusing only on scoring,^{13,19,20} pose optimization,^{21–23} or screening.²⁴ Specifically, the scoring task is to predict the binding affinity of protein–ligand complexes, and the screening task is to classify different compounds into true binders and non-binders. Contrary to the common expectation that a model with high accuracy in binding affinity scoring will also have high accuracy in virtual screening, the performance of these two tasks is often at odds because deep learning models tend to learn exclusive (rather than generalizable) features to perform best at each task. For example, models for predicting binding affinity trained only on crystal structures performed well at scoring crystal or near-native structures but struggled with tasks such as identifying specific binders to a target protein among diverse molecules or evaluating computer-generated structures as required in virtual screening.²⁵ Meanwhile, models that employ a Δ -learning strategy with computer-generated data^{24,26} or target the binding pose optimization^{21,22} have shown improved performance in virtual screening but failed to rank the binding affinities of different

^a Department of Chemistry, KAIST, 291 Daehak-ro, Yuseong-gu, Daejeon, 34141, Republic of Korea. E-mail: wooyoun@kaist.ac.kr

^b HITS Incorporation, 124 Teheran-ro, Gangnam-gu, Seoul, 06234, Republic of Korea.

^c AI Institute, KAIST, 291 Daehak-ro, Yuseong-gu, Daejeon, 34141, Republic of Korea.

[†] Electronic Supplementary Information (ESI) available: [details of any supplementary information available should be included here]. See DOI: 00.0000/00000000.

protein–ligand complexes adequately. These challenges underscore the difficulty in designing a versatile PLI prediction model that can effectively handle diverse tasks.

Designing a versatile deep learning-based PLI prediction model performing well on both scoring and screening is challenged by the low generalizability of the model, which is mainly due to the lack of well-curated structure–affinity data.^{27–29} This challenge persists despite the gradually increasing availability of binding structure data from experiments.³⁰ To overcome this hurdle, one can impose a generalizable inductive bias throughout various tasks into the model. In the previous study, we have shown that incorporating the physics of non-covalent molecular interaction as an inductive bias improves the generalization of a deep learning-based PLI prediction model.³¹ In addition, data augmentation strategies can mitigate the problem of the lack of structure–affinity data. Previous approaches adopted data augmentation strategies by training the model with docking-generated structures to predict the binding affinity of non-binding structures to be lesser than that of experimental structures.^{32,33} These strategies are based on the physical intuition that highly divergent structures of cognate ligands or structures with non-cognate ligands for a given target would have weaker binding affinities than a crystal structure. However, models trained only with such augmented data have exhibited a relative decrease in scoring performance, diminishing their utility for this particular task.^{31,34}

In this light, we propose a versatile deep learning-based PLI prediction model for both scoring and screening tasks by improving its generalization ability with physics-based inductive bias and data augmentation strategy. Along with the previous data augmentation strategies, we synthesize near-native structures that are energetically and geometrically similar to crystal structures to consider their limited resolution and dynamic nature. The model is then trained to predict the binding affinity of these structures to be the same as the experimental value, effectively recognizing that these structures lie on the same local minima as crystal structures. As a result, PIGNet2, which is based on the physics-informed graph neural network from our previous work,³¹ showed significantly enhanced scoring and screening performance.

To demonstrate the potential applicability of PIGNet2 in scoring and screening tasks, we evaluated it against various benchmarks. We used the CASF-2016 benchmark³⁵ to compare the overall performance on scoring and screening. Following that, we also employed the DUD-E benchmark³⁶ to evaluate the screening performance in more detail. As a further assessment of the scoring performance of our model, we adopted a derivative benchmark, a structure–affinity dataset for derivative compounds corresponding to various targets, which was provided by Wang *et al.*³⁷

On the CASF-2016 benchmark, PIGNet2 showed both scoring and screening performances comparable to other deep learning-based PLI prediction models specifically designed for one of scoring or screening, demonstrating its potential as a versatile PLI prediction model. Further analysis of data augmentation strategies with the DUD-E benchmark confirmed that adding our new data augmentation strategy to previous strategies improves screening performance by identifying near-native conformations more reli-

ably. In addition, PIGNet2 also achieved remarkable performance on the derivative benchmark, surpassing the scoring accuracy of MM-GB/SA and comparable to a state-of-the-art model designed exclusively for this purpose. Thus, our approach provides a viable solution for a versatile deep learning model that can be used for hit identification and lead optimization in the early stage of drug discovery.

2 Methods

2.1 PDBbind dataset

The PDBbind dataset,³⁸ which comprises protein–ligand binding complex data curated from the Protein Data Bank (PDB),³⁹ is divided into general, refined, and core sets based on the strictness of the curation. The core set is subjected to the most rigorous curation criteria, thus including representative entities with respect to the target protein. A growing trend among recent PLI prediction models is to exploit the general set in order to leverage a larger pool of crystal structures for training.^{32,33} This approach was inspired by previous work demonstrating that using the larger general set can improve the performance of PLI prediction models when compared to the refined set.⁴⁰

In our study, however, we employed the refined set to carry out data augmentation for all the proteins and ligands with limited computational resources. This may indicate that our model still has room for improvement by expanding the number of crystal structure data with the general set. Of the 5,312 complexes present in the refined set, we omitted the core set included in the CASF-2016 benchmark³⁵ and redundant complexes. As a result, we ended up with a training set of 5,046 complexes and a test set of 266 complexes.

2.2 Data augmentation strategies

In this section, we present our novel positive data augmentation (PDA) strategy in conjunction with various negative data augmentation (NDA) strategies: re-docking, random-docking, and cross-docking data augmentation.

2.2.1 Positive data augmentation

Recent deep learning-based PLI prediction models commonly utilize crystal structures and docked structures from NDA as input, where the unnatural NDA-generated structures get substantially more abundant than crystal structures. We hypothesize that this data imbalance potentially impedes the discrimination between near-native and unnatural (or unstable) structures, thereby degrading the performance of binding affinity prediction for crystal or near-native structures. Since each crystal structure is a single snapshot of conformations around local minima of a potential energy surface, treating near-native structures as true binders may implicitly integrate the conformational ensemble effect into the PLI prediction model. In this light, we introduced a novel data augmentation strategy, PDA, designed to generate energetically and geometrically near-native conformations for any given complex structure.

For PDA, we first generated 1,000 conformations of each ligand using the ETKDG conformer generation method.⁴¹ We optimized

those structures using the universal force field (UFF)⁴² and Merck molecular force field (MMFF).⁴³ This can yield a maximum of 3,000 data points for each complex. Next, the resulting structures were aligned to the ligand’s pose in the crystal. Finally, the structures are minimized using the Smina docking software,⁴⁴ a forked version of AutoDock Vina,⁴⁵ to avoid clashes. We then selected structures that satisfy two criteria: (1) a ligand root mean square deviation (RMSD) less than 2 Å compared to the crystal structure and (2) a mean absolute error less than 1 kcal/mol between the Smina scores of the crystal structure and the generated structures. The latter criterion aims to select structures energetically similar to the near-native structure, in addition to the former, the geometric criterion that is more generally used. While the scoring function of Smina only approximates the PLI potential energy surface (PES), it is rational to regard structures with similar scores in a confined range as energetically near-native on the actual PES considering the continuity of energy. Finally, to remove highly similar structures that can be considered duplicates, we additionally pruned the generated structures so that the RMSD between every pair of the generated structures is greater than 0.25 Å. Along with the above, structures generated by re-docking crystal structures using Smina were also used.

2.2.2 Negative data augmentation

The negative data augmentation strategies mostly follow the methods outlined in our previous work,³¹ with additional guidelines to generate non-binding structures more rigorously. First, the re-docking data augmentation generates structures by docking ligands into a cognate target and then extracting unstable structures. Based on the fact that crystal structures are stable binding poses, one can infer that ligand structures that deviate greatly from the crystal structure will be highly unstable. Thus, we used docking-generated structures with the ligand RMSD greater than 4 Å compared to the corresponding crystal structure. Second, cross-docking data augmentation uses the idea that a non-cognate protein–ligand pair is less likely to form a bound complex. To implement this, we grouped proteins based on a protein sequence similarity of 0.4 using the cd-hit software.^{46,47} Then, pairs of different protein clusters were sampled, and for each pair of clusters, proteins from one cluster were docked with ligands from the other cluster to generate structures of non-cognate protein–ligand pairs. Lastly, the random-docking data augmentation strategy assumes that an arbitrarily chosen molecule is unlikely to be a true binder to a given protein by chance. We generated the corresponding structures by docking a random molecule from the IBS molecule dataset⁴⁸ to each protein. For all the negative data augmentation strategies, we used Smina for docking and structure minimization and the DockRMSD⁴⁹ software for calculating the ligand RMSD.

2.3 Data preprocessing

To convert crystal structures and the simulated structures into inputs for the PLI prediction model, we carried out additional preprocessing steps. We protonated all the protein structures with the Reduce software.⁵⁰ For the ligands, we protonated them at pH 7.4 using Dimorphite-DL.⁵¹ Water and hydrogens were removed

from the complexes. As a final step, only the protein residues containing heavy atoms within 5 Å or less from the ligand were extracted and used as the protein pocket. We used RDKit,⁵² Open Babel,⁵³ and PyMOL⁵⁴ throughout. A detailed breakdown of the training and test sets, derived through each data augmentation, is presented in Table 1.

Table 1 Number of data points generated from each data augmentation strategy

Data augmentation strategy	Training set	Test set
PDA	375,184	21,377
NDA (re-docking)	254,163	12,109
NDA (cross-docking)	503,073	26,470
NDA (random-docking)	957,775	50,496

2.4 Model architecture

PIGNet2 incorporates the model architecture and physics terms from our previous work³¹ except for the initial atom features. Refer to ESI† for the modified initial atom features of PIGNet2.

PIGNet2 works as follows: preprocessed pocket and ligand structures, in conjunction with input features, are first passed through a feedforward network and then through a gated graph attention network. The resulting pocket and ligand features are then passed through an interaction network, which allows the embedding of additional information from the counterpart. Following this, the pocket and ligand features are concatenated, facilitating the calculation of the contribution of physics terms to the binding affinity based on these unified features.

The total binding affinity E^{pred} predicted by the model is the sum of all intermolecular atom pairwise energies consisting of four terms: E^{vdW} , E^{Hbond} , E^{Metal} , and $E^{\text{Hydrophobic}}$. Each of them represents intermolecular van der Waals (vdW), hydrogen bond, metal–ligand, and hydrophobic interactions, respectively. In order to incorporate the effect of entropy as regularization, the total energy is divided by T^{rot} , a term proportionate to the number of rotatable bonds of the ligand. The equation of the total energy is as follows:

$$E^{\text{pred}} = \frac{E^{\text{vdW}} + E^{\text{Hbond}} + E^{\text{Metal}} + E^{\text{Hydrophobic}}}{T^{\text{rot}}}. \quad (1)$$

One feature of our current model that differs from the previous is the inclusion of the Morse potential instead of the Lennard-Jones potential for E_{vdW} . The ability of PIGNet2 to score the binding affinity of crystal structures or to clearly distinguish between active and decoy molecules is highly dependent on the modeling of the vdW potential well. For example, an overly broad potential well could result in the prediction of a degree of interaction even for atom pairs that are too far apart to contribute significantly to the interaction, resulting in predicting inherently unstable structures to be stable. On the other hand, an excessively narrow potential well could lead to the prediction of repulsive vdW interactions for atom pairs that are appropriately close, resulting in predicting unstable energies for them. The correct form of the potential well is, therefore, critical for accurate predic-

tion. Thus, directly adjusting the potential well offers significant advantages in the design and evaluation of deep learning-based physics-informed PLI prediction models. However, the Lennard–Jones potential possesses insufficient flexibility to freely adjust the width of the potential well, which was our reason to introduce the derivative loss in the previous work.³¹ As a more direct and precise alternative, we chose to use the Morse potential, which allows for explicitly controlling the potential well. The formula for the Morse potential is given below:

$$E^{\text{vdW}} = w((1 - e^{-a(d-r)})^2 - 1), \quad (2)$$

where d denotes the interatomic distance and r is the sum of vdW radii of the atom pair. Note that we used r as the pairwise sum of vdW radii instead of the pairwise *corrected* sum of vdW radii from the previous study³¹ not only for the Morse potential but also for all the other physics terms. The coefficient a modulates the width of the potential well, while w affects the depth of the potential well. For the case where d is greater than r , the coefficient a is predicted by the neural network, while for the opposite case, it is set as a hyperparameter, with a value of 2.1 chosen for PIGNet2.

2.5 Training setup

2.5.1 Loss function

PIGNet2 employs various loss functions to optimize the model through the learning objectives of each data augmentation strategy. Specifically, the PDA and crystal structures, acting as near-native structures, are trained using the mean squared error loss. This approach induces the model to precisely predict the experimental binding affinity for near-native structures as well as crystal structures to inform the model that both structures from PDA and crystal structures belong to the same local minima in PES. In contrast, for data exhibiting significant structural deviations from the crystal structure, which is derived from the re-docking process of NDA, we employed a hinge loss to predict a lower binding affinity than that of the crystal structure. Lastly, we applied a hinge loss for cross-docking and random-docking data augmentation in another way. This helps to predict binding affinities for the structures higher than a criterion of -6.8 kcal/mol, consistent with the assumption that these structures are unlikely to have a binding interaction. Altogether, the total loss function is a weighted sum of all the losses above. A more detailed description of the loss function is shown in the ESI.†

2.5.2 Training procedure

During the training with PDA, we merged the PDA and crystal structures into a single dataset. Meanwhile, during the training with NDA, we set the number of data for each dataset that the model learns per epoch to be equal. Throughout the training, we used a batch size of 64, a learning rate of 0.0004, and a dropout ratio of 0.1. We used a single RTX A4000 GPU for all training and inference. Finally, all our results are an ensemble of predictions from four models, each initialized with a different random seed.

3 Results and discussion

3.1 Performance on CASF-2016 benchmark

3.1.1 CASF-2016 benchmark

To demonstrate the versatility of PIGNet2 for broad applications, we employed the well-established CASF-2016 benchmark.³⁵

The CASF-2016 benchmark was carefully curated from 285 protein–ligand complexes in the PDBbind core set. This benchmark provides a comprehensive set of four metrics: scoring power, ranking power, docking power, and screening power. Each of these metrics serves a unique purpose in assessing PLI prediction models.

The metrics fall into two main categories. The first category evaluates the ability of the model to predict binding affinity for crystal structures. The second category evaluates the ability of the model to distinguish true-binding structures from a variety of computer-generated structures. Scoring power and ranking power fall into the first category, and docking power and screening power fall into the second category. The four powers together comprehensively evaluate the model’s performance in different aspects of PLI prediction.

To be specific, scoring power evaluates the ability of the model to predict the binding affinity of protein–ligand crystal structures and is assessed using the Pearson correlation coefficient R . Ranking power measures the ability of the model to rank the binding affinities of protein–ligand complexes grouped by protein similarity. It is evaluated using the Spearman rank correlation coefficient ρ . Docking power assesses the ability of the model to identify near-native structures from computer-generated decoy structures. The metric is evaluated based on a top N success rate, SR_N , where a case is considered successful if at least one of the top N predicted structures for each complex has a ligand root mean square deviation (RMSD) of less than 2 Å when compared to the crystal structure. Finally, screening power evaluates the ability of the model to identify cognate protein–ligand complexes that can form a binding interaction among the vast amount of non-cognate protein–ligand complexes in cross-docking scenarios. The screening power is assessed with the top $\alpha\%$ enrichment factor, $\text{EF}_{\alpha\%}$, which is a measure of the ratio of active molecules included in the top $\alpha\%$ model predictions to the total number of active molecules, defined as follows:

$$\text{EF}_{\alpha\%} = \frac{\text{NTB}_{\alpha}}{\text{NTB}_{\text{total}} \times \alpha}, \quad (3)$$

where NTB_{α} is a number of active molecules in top $\alpha\%$ and $\text{NTB}_{\text{total}}$ is total number of active molecules in overall dataset. Along with $\text{EF}_{\alpha\%}$, we also report the top $\alpha\%$ success rate, $\text{SR}_{\alpha\%}$, which measures the success rate of finding the best binder among the top $\alpha\%$ top-ranked structures for all targets.

3.1.2 Baseline models

We selected several task-specific deep learning-based PLI prediction models as baselines for comparative studies. These models differ in their prediction targets during training and inference, tailored to excel in their respective objective tasks. Thus, the models are categorized based on their prediction targets: distance likeli-

Table 2 Results on the CASF-2016 benchmark. EF_{1%}, SR_{1%}, *R*, and ρ are top 1% enrichment factor, success rate, Pearson correlation coefficient, and Spearman rank correlation coefficient, respectively. The results of all baseline PLI prediction models are originated from their respective literature. For PIGNet2, we report the results of 4 randomly initialized model ensemble trained with both positive data augmentation and negative data augmentation. For each metric, the best performance is shown in bold and the second best performance is underlined

Model	Prediction target	Screening power		Docking power	Scoring power	Ranking power
		Average EF _{1%}	SR _{1%}	SR _{1%}	<i>R</i>	ρ
DeepDock ²¹	Distance likelihood	16.4	<u>43.9%</u>	89.1%	0.460	0.425
RTM-Score ²²	Distance likelihood	28.0	66.7%	97.3%	0.455	0.529
OnionNet-SFCT(Vina) ²⁴	Δ binding affinity	15.5	-	<u>93.7%</u>	0.428	0.393
Δ -AEScore ²⁶	Δ binding affinity	6.16	19.3%	85.6%	0.740	0.590
OnionNet-2 ¹⁹	Exact binding affinity	-	-	-	0.864	-
AEScore ²⁶	Exact binding affinity	-	-	35.8%	<u>0.83</u>	0.64
AK-score ¹³	Exact binding affinity	-	-	36.0%	0.812	0.670
Sfcnn ²⁰	Exact binding affinity	-	-	34.0%	0.795	-
PIGNet2	Exact binding affinity	<u>24.9</u>	66.7%	93.0%	0.747	<u>0.651</u>

hood, Δ binding affinity, and exact binding affinity, to differentiate the results from previous approaches better. Our model, PIGNet2, falls into the category that directly predicts exact binding affinity.

Two baseline models, DeepDock²¹ and RTMScore,²² primarily aim to optimize protein–ligand structures. Instead of predicting binding affinities, these models target the distance likelihood of given structures by utilizing a mixture density network⁵⁵ to model the statistical potential of protein–ligand structures.

OnionNet-SFCT²⁴ and Δ -AEScore,²⁶ on the other hand, estimate the final energy by linearly combining correction terms to the Autodock Vina⁴⁵ scores. These methods incorporate various computer-generated structures in their training process to enhance performance in virtual screening tasks.

Finally, baseline models that directly predict accurate binding affinity include AK-score,¹³ Sfcnn,²⁰ OnionNet-2,¹⁹ and AEScore.²⁶ AK-score and Sfcnn use 3D convolutional neural networks (CNN), while OnionNet-2 uses a 2D feature map with a 2D CNN. AE-score, which differs from the CNN structure, predicts binding affinity using a feedforward neural network based on the atomic environment vector representation. By including these different models in our comparison, we can thoroughly evaluate the relative performance and robustness of PIGNet2.

3.1.3 Performance of PIGNet2

The performance of PIGNet2, along with all known results from the baseline models, is shown in Table 2. Models that predict distance likelihoods, such as DeepDock and RTMScore, show strong performance in distinguishing between computer-generated and crystal structures, as evidenced by their impressive docking and screening power. However, their ability to predict or compare the binding affinity of crystal structures is limited. It is natural because their distance likelihood computation can only infer the relative stability of conformations of a single protein–ligand complex. This makes it difficult to compare different protein–ligand complexes of stable structures, mirroring the limitations of traditional knowledge-based PLI prediction models that utilized statistical potentials.

On the other hand, models that focus on accurate regression

of binding affinities, which have been the subject of consistent research, generally demonstrate their superior performance in scoring and ranking. Nevertheless, their performance on virtual screening-related metrics lags behind those predicting distance likelihoods. Prime examples of such models include AEScore and OnionNet-2, and they have attempted to compensate for the poor screening performance by introducing various computer-generated structures and Δ -learning. However, although the resulting OnionNet-SFCT and Δ -AEScore enhanced docking and screening power, their scoring and ranking power were significantly reduced. This trend was particularly pronounced for OnionNet-SFCT, whose scoring and ranking performance approached that of models predicting distance likelihood, indicating that designing versatile deep learning-based PLI prediction models is challenging even with data augmentation and Δ -learning.

PIGNet2 aimed to achieve high rankings in all performance criteria from both virtual screening and binding affinity scoring perspectives by using a physics-informed graph neural network coupled with various data augmentation strategies. Contrary to the results of the aforementioned models, PIGNet2 delivered high performance across all CASF-2016 benchmarks. In particular, in the context of screening performance, PIGNet2 demonstrated competitive performance comparable to RTMScore, the state-of-the-art model. It also achieved similar results to DeepDock and RTMScore in their primary objective — pose optimization — as reflected in docking power. Simultaneously, PIGNet2 also attained scoring and ranking power comparable to OnionNet-2, AEScore, AK-score, and Sfcnn, all of which aim to score the binding affinity of crystal structures accurately. PIGNet2 also outperformed in all metrics, compared to OnionNet-SFCT and Δ -AEScore, which aim to improve docking and screening performance by introducing the Δ -learning strategy. These results suggest that PIGNet2, trained with data augmentation strategies, can serve as a versatile deep learning-based PLI prediction model.

3.2 Performance on classifying active and decoy compounds

While the CASF-2016 screening benchmark is well-designed, it slightly differs from the real-world virtual screening scenario due to relatively fewer numbers of actives and decoys. In this light, we utilized the DUD-E benchmark to evaluate the performance of PIGNet2 in situations resembling real-world virtual screening scenarios.

3.2.1 DUD-E benchmark

The DUD-E benchmark³⁶ is a widely used benchmark for validating the virtual screening performance of a PLI prediction model. Compared to the CASF-2016 benchmark, this benchmark is more similar to the real-world scenario where a limited number of active structures need to be identified among a vast pool of decoys, as it includes dozens of actives and thousands to tens of thousands of decoys for a single target. While some studies have criticized the DUD-E benchmark for its lack of generalizability,^{16,56} most of these investigations are based on the results of both training and inference conducted using the DUD-E benchmark. We expect that generalizability issues may be attenuated in our case because our model, PIGNet2, was not trained directly on the DUD-E training set. Since the DUD-E benchmark does not provide structure data for ligands, we manually created initial conformations with ETKDG followed by UFF minimization. Then we selected the most stable structure generated by the Smina docking simulation.

To evaluate the screening performance of PIGNet2 and to conduct a comparative assessment with other deep learning-based PLI prediction models, we selected the top $\alpha\%$ enrichment factor as our primary benchmark metric, consistent with the CASF-2016 screening benchmark. Additionally, to conduct an ablation study on data augmentation in the context of screening performance, we utilized the Kullback–Leibler (KL) divergence, D_{KL} .⁵⁷ The KL divergence measures the extent to which two distributions diverge. Here, we employed this metric to measure the deviation between the predicted binding affinity distributions of actives and decoys. Given the predicted value distribution for actives, D_{active} , and the predicted value distribution for decoys, D_{decoy} , the KL divergence is represented by the following equation:

$$D_{KL}(D_{\text{active}}||D_{\text{decoy}}) = \sum_{x \in \mathcal{X}} D_{\text{active}}(x) \log \left(\frac{D_{\text{decoy}}(x)}{D_{\text{active}}(x)} \right). \quad (4)$$

The KL divergence always has a positive value, and the higher its value, the greater the deviation between the D_{active} and D_{decoy} distributions.

3.2.2 Baseline models

We adopted three deep learning-based PLI prediction models for the comparative analysis. OnionNet-SFCT is a model that predicts correction terms for the scoring function of docking programs, as previously mentioned in Section 3.1.2. For the comparison, we chose the model that uses a scoring function correction term for Autodock Vina.⁴⁵ Also, the previously introduced RTMScore predicts the distance likelihood and is one of the best PLI prediction models within screening performance. Gnina is a 3D CNN-based model that, similar to PIGNet2, is trained using various data augmentation strategies and tasks. Gnina offers several PLI predic-

tion models that mainly target virtual screening. Here, we chose the Dense (Affinity) model, namely Dense, which showed state-of-the-art results among exact binding affinity prediction models in previous research.⁵⁸

3.2.3 Performance of PIGNet2

For the evaluation of the screening performance of PIGNet2, we rescored the docking-generated structures of actives and decoys for a given target. Figure 1(A) shows the average DUD-E top 1% enrichment factor, $EF_{1\%}$, for PIGNet2 and the baseline models. Although the screening performance of PIGNet2 appears inferior to RTMScore, it should be noted that the latter is difficult to use in scoring tasks. However, compared to the other PLI prediction models, PIGNet2 demonstrated superior screening performance. Specifically, it achieved a 31.9% performance improvement over Gnina. We emphasize that although both OnionNet-SFCT and Gnina are models developed focusing on virtual screening, PIGNet2 showed superior screening performance while achieving high scoring performance. Moreover, considering that Gnina showed better screening performance than traditional scoring functions such as Vina,⁴⁵ Vinardo,⁵⁹ and RFScore-4,⁶⁰ it is evident that PIGNet2 exhibits better screening performance even when compared to traditional PLI prediction models.

3.2.4 Ablation study on data augmentation strategies

To elucidate the impact of our proposed data augmentation strategies on screening performance, we conducted ablation studies based on $EF_{1\%}$ results of models trained with and without NDA and PDA. This is detailed in Figure 1(B). Firstly, we observed that a model solely trained on crystal structures without both PDA and NDA exhibited no increase in $EF_{1\%}$ after incorporating PDA. Since PDA helps the model to observe near-native conformations of binders, rather than discriminating diverse decoys as NDA does, this result could be expected.

However, adding PDA to a model already improved by NDA further improved its performance compared to a model trained with NDA alone. The observation that the gain in $EF_{1\%}$ from the introduction of PDA is more prominent in the NDA-only model than in the model without both PDA and NDA may suggest that PDA can differentiate more of the active and decoy structures that are rendered indistinguishable in the NDA-only model than in a model trained without any data augmentation. This suggests that PDA can effectively regularize the potential biases introduced by NDA, enhancing the model to discriminate between actives and decoys. Ultimately, when we compared the $EF_{1\%}$ of the model trained without any data augmentation and the model trained with all data augmentation methods, the result of the latter was more than twice higher than that of the former.

Next, we plotted the distribution of predicted binding affinity for actives and decoys in the DUD-E benchmark, as shown in Figure 1(C), to analyze how the use of each data augmentation leads to an improvement in $EF_{1\%}$. The model trained without any data augmentation is on the left, the one trained with only NDA is in the middle, and the one trained with both NDA and PDA is on the right. Without data augmentation, the majority of the active and decoy distributions overlap. However, the overlap decreases

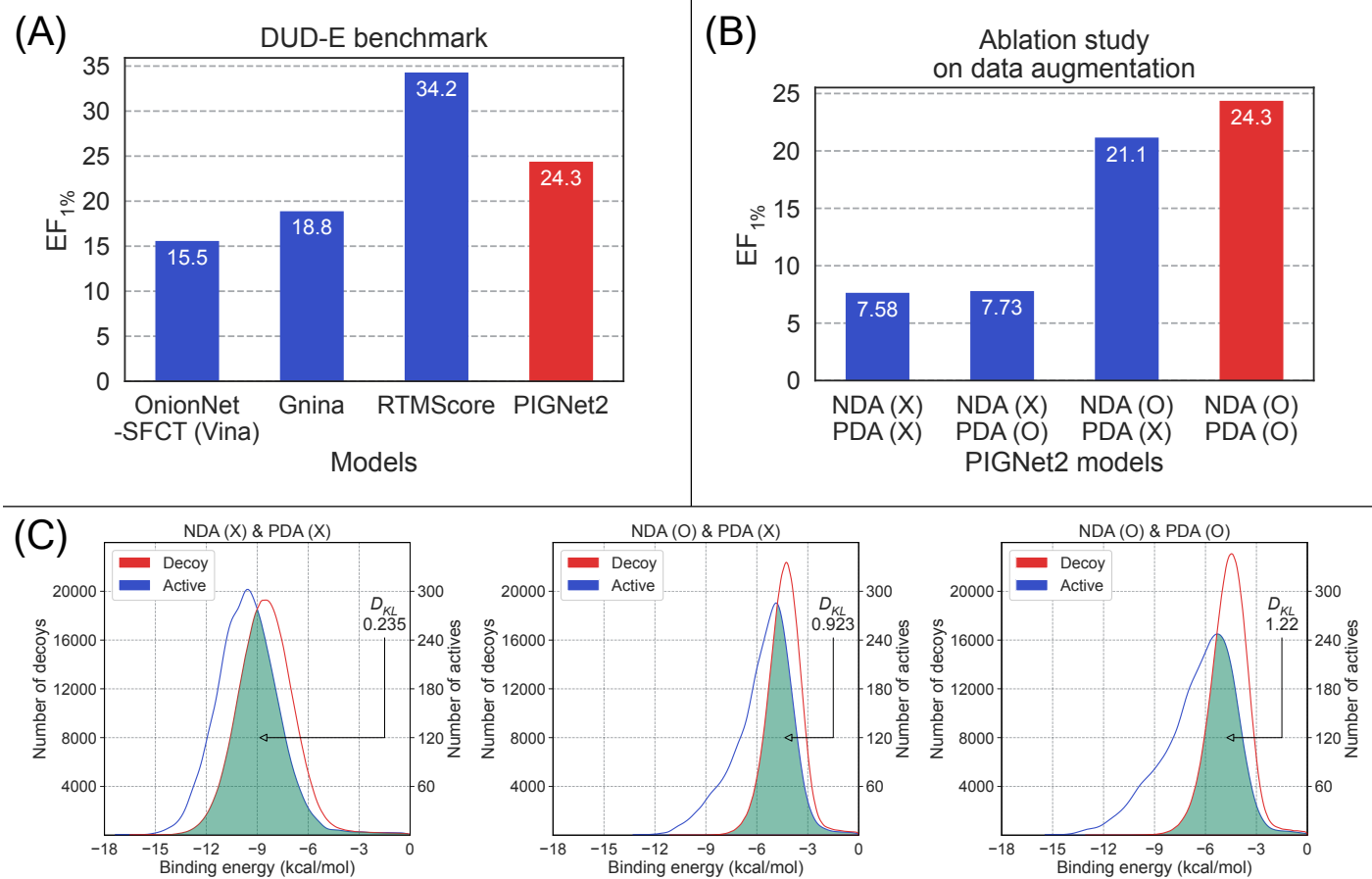


Fig. 1 Results for the DUD-E benchmark. EF_{1%} is top 1% enrichment factor. (A) Comparison between baseline models and PIGNet2 in terms of the EF_{1%}. (B) Ablation study about data augmentation strategies for PIGNet2 on the enrichment factor of the DUD-E benchmark. Each labels on x-axis means the data augmentation strategies used for training PIGNet2. For example, NDA (O) means the model trained with NDA and PDA (X) means the model trained without PDA. The red bar shows PIGNet2 model with the best performance. (C) Ablation study about data augmentation strategies for PIGNet2 on predicted distributions of actives and decoys of the DUD-E benchmark. Three models are compared: the model trained without any data augmentation strategies (left), the model trained with NDA alone (middle), and the model trained with both NDA and PDA (right). In each sub-figure, the green colored region is an overlap between the distributions of actives and decoys.

when data augmentation is employed, implying that the active and decoy distributions diverge more significantly.

Interestingly, the distribution of predictions from the model with NDA shifted to the right compared to the model without any data augmentation. This could be associated with the hinge loss used in most models that employ NDA, which results in lower binding affinity predictions for some active molecules, consequently weakening both the screening and scoring performance. When PDA was additionally employed in the training process of the model trained with only NDA, there was still some shift in the active distribution compared to the model without any data augmentation. However, this shift was less than that of the model trained with only NDA, and the overall distributions of actives and decoys are more clearly distinguished.

Moreover, the number of actives in high binding affinity regions relative to decoys, which is the left tail of the blue-colored active distribution, increased progressively from left to right in Figure 1(C). This result directly accounts for the increase in EF_{1%}, as EF_{1%} measures the proportion of active molecules in the top 1%

of predictions. Therefore, the relative number of actives in high binding affinity regions increased the EF_{1%} value.

To complement the analysis above, we evaluated the separation between the predicted binding affinity distributions of active and decoy instances in terms of D_{KL} as a result of data augmentation. Despite not being a direct assurance of high EF_{1%}, a greater D_{KL} can be suitably considered as a strong indicator positively associated with a high EF_{1%}. The rationale behind this connection lies in the fact that a larger D_{KL} signifies a greater distinction between active and decoy distributions, thus enhancing the likelihood of identifying more actives in regions characterized by higher binding affinities compared to decoys. As depicted in Figure 1(C), the D_{KL} of the model without any data augmentation, the NDA-only model, and the model with both NDA and PDA are 0.235, 0.923, and 1.22, respectively. In summary, we can conclude that adding NDA and PDA can better separate the predicted binding affinity distributions of active and decoy.

Table 3 Results on the derivative benchmark, where R means Pearson correlation coefficient. The results of the models with * are from Wang *et al.*³⁷ while remained models were calculated in this work. For PIGNet2, we report the results of 4 randomly initialized models ensemble trained with both positive data augmentation and negative data augmentation. The best performance is shown in bold.

Model	Performance	Systems							
	Average R	BACE	CDK2	JNK1	MCL1	p38	PTP1B	Thrombin	Tyk2
MM-GB/SA ^{37*}	0.40	-0.40	-0.53	0.65	0.42	0.66	0.67	0.93	0.79
Glide SP ^{37*}	0.29	0.00	-0.56	0.24	0.59	0.14	0.55	0.53	0.79
Smina ⁴⁴	0.25	-0.48	0.10	-0.060	0.24	0.52	0.70	0.72	0.24
RTMScore ²²	-0.28	-0.19	0.68	-0.30	-0.67	-0.38	-0.42	-0.81	-0.14
OnionNet-SFCT (Vina) ²⁴	0.023	-0.48	-0.68	-0.59	0.29	0.50	0.66	0.71	-0.23
Sfcnn ²⁰	0.084	-0.24	0.044	-0.65	0.12	0.58	0.58	0.041	0.20
PIGNet2	0.64	0.42	0.77	0.36	0.78	0.60	0.76	0.83	0.61

3.3 Performance on ranking structurally similar compounds

Selecting molecules with higher binding affinity to a target among plenty of similar derivatives is an important task during hit-to-lead and lead optimization. For this purpose, one can rank the relative binding affinities of similar derivative molecules. However, this remains challenging due to issues such as activity cliffs, where small changes in the molecule can result in significant changes in activity. To further demonstrate the exceptional performance of PIGNet2 in predicting binding affinity, especially when compared to other PLI prediction models, we evaluated the predictive performance of the others on a derivative benchmark.

3.3.1 Derivative benchmark

The derivative benchmark is a dataset initially proposed by Wang *et al.*³⁷, composed of 199 data, comprising a number of derivatives and their corresponding experimental binding energies and Free Energy Perturbation (FEP) calculation results for eight target systems. We leveraged this data to evaluate further the ability of methods to predict binding affinity. Structures in the provided data are initial structures for FEP simulations. In each target system, the structures of numerous derivatives are aligned to a fixed protein structure. In this context, the ability to predict the relative binding affinity among similar derivatives for a given target is assessed by calculating the Pearson correlation coefficient, R , of each target system.

3.3.2 Baseline models

Wang *et al.*³⁷ compared the binding affinity prediction performance of several physics-based methods: FEP, Molecular Mechanics/Generalized Born and Surface Area Solvation (MM-GB/SA), and Glide SP. Here, we aimed to evaluate methods with comparable computational costs, excluding FEP due to its high computational cost despite its high accuracy. The remaining MM-GB/SA and Glide SP results are computed from a single snapshot of a given complex structure. In particular, Glide SP is a widely-used traditional scoring function. We also introduce another traditional scoring function, Smina,⁴⁴ which is used for minimization of initial structures.

Moreover, to compare with the deep learning-based PLI prediction models, we selected Sfcnn,²⁰ OnionNet-SFCT (Vina),²⁴ and

RTMScore.²² These models are all deep learning-based PLI prediction models with different prediction targets previously used as baseline models in the CASF-2016 benchmark. For a more rigorous performance evaluation on the derivative benchmark, we present the results for reproducible models. In summary, MM-GB/SA, Glide SP, and Smina can be categorized as traditional scoring functions, while RTMScore, OnionNet-SFCT (Vina), and Sfcnn are deep learning-based PLI prediction models.

Except for OnionNet-SFCT (Vina), which rescores docked structures from AutoDock Vina, the results for all other models were computed using structures minimized by the Smina. We performed structure minimization because the original structures were aligned to particular target proteins, occasionally resulting in excessively small intermolecular atomic distances that we aimed to exclude.

3.3.3 Performance of PIGNet2

The overall performance of all models on the derivative benchmark is presented in Table 3. Notably, PIGNet2, trained using all data augmentation strategies, demonstrates superior performance compared to traditional scoring functions. Glide SP and Smina, the traditional scoring functions, showed anticorrelated results for specific systems such as BACE and CDK2. Given that the former was developed for virtual screening, its limited performance in binding affinity scoring was expected. Remarkably, PIGNet2 outperforms MM-GB/SA, which is utilized in molecular dynamics and is expected to be more accurate than conventional scoring functions. Even for the BACE and CDK2 systems where MM-GB/SA displayed anticorrelated tendencies, PIGNet2 shows a correlated trend.

Since the derivative benchmark requires accurate prediction of the binding affinity of the structurally similar derivatives for the same target protein, it is a much more challenging task than scoring and ranking in the CASF-2016 benchmark, where protein-ligand complexes vary significantly. In this context, RTMScore, which targets pose optimization, showed anticorrelated results in almost all systems albeit its impressive screening performance. This result suggests that the ability of distance likelihood-based PLI prediction models to predict binding affinities for different protein-ligand complexes is limited. OnionNet-SFCT (Vina),

Table 4 Ablation studies for PIGNet2 on the derivative benchmark, where R means Pearson correlation coefficient. For each model, we report the results of 4 randomly initialized models ensemble. The best performance is shown in bold.

Model	Data augmentation		Performance Average R	Systems							
	Negative	Positive		BACE	CDK2	JNK1	MCL1	p38	PTP1B	Thrombin	Tyk2
PIGNet2	X	X	0.50	-0.16	0.36	0.21	0.71	0.67	0.64	0.82	0.74
PIGNet2	X	O	0.54	0.23	0.61	0.33	0.69	0.64	0.76	0.66	0.37
PIGNet2	O	X	0.39	0.085	-0.29	0.25	0.75	0.45	0.32	0.82	0.71
PIGNet2	O	O	0.64	0.42	0.77	0.36	0.78	0.60	0.76	0.83	0.61

developed based on Δ learning focusing on virtual screening, showed similar results. Surprisingly, Sfcnn, designed to score binding affinities accurately and has the exact binding affinity as its prediction target, performed only marginally better than OnionNet-SFCT (Vina) and poorer than traditional scoring functions. This unsatisfactory performance may be because Sfcnn, as a 3D CNN-based model, was trained exclusively on crystal structures and thus struggled to accurately score structures optimized by Smina. Notably, PIGNet2 showed superior results compared to other deep learning-based PLI prediction models for all systems.

Furthermore, the performance of PIGNet2 in the derivative benchmark, especially in terms of average R , is surprisingly close to that of PBCNet⁶¹ (0.65), a model exclusively designed for predicting the relative binding affinity of two given molecules. This observation underscores the competitive position of PIGNet2 within the derivative benchmark, particularly when compared to models designed for predicting relative binding affinities, given that the extraordinary performance of the PBCNet outperforms other deep learning-based PLI prediction models. Remarkably, the superior performance of PIGNet2 persists even when predicting the binding affinity for each complex, as opposed to the relative value, thereby demonstrating the effective binding affinity prediction performance of PIGNet2, which can also make it applicable to other tasks such as virtual screening.

3.3.4 Ablation study on data augmentation strategies

To understand the impact of PDA on scoring performance, we conducted an ablation study for PIGNet2 on the derivative benchmark. Table 4 provides a comprehensive comparison of the influence of NDA and PDA on the scoring performance of PIGNet2 across multiple datasets, with the effect of PDA particularly highlighted in terms of the average Pearson correlation coefficient (R). An initial comparison between the model trained without any data augmentation and the one trained solely with NDA reveals a slight decrease in the overall average R . Notably, we can observe an inversion of the correlation for CDK2 due to the use of NDA, which negatively affects the scoring performance, while changes in other systems remain relatively negligible.

However, when PDA is incorporated alongside NDA, the model regains a high correlation for CDK2. Moreover, the model trained exclusively with PDA alone outperforms the model trained without any data augmentation in terms of scoring performance. These results suggest a significant impact of PDA in mitigating potential biases that could occur when training with only crystal structures and NDA alone, thereby significantly improving the

scoring performance of PIGNet2.

The incorporation of PDA typically manifests itself as either maintaining or positively affecting most systems except Tyk2, with some systems showing particularly profound improvements. In this context, we have visualized the affinity prediction results for CDK2, the target for which the introduction of PDA led to the most significant performance improvements, in Figure 2. In particular, the figure highlights a drastic reversal of the correlation trend from -0.29 to 0.77 upon incorporating PDA into a model initially trained on NDA alone. This transformation may illustrate the immense potential of PDA in enabling a deep learning-based PLI prediction model to improve scoring performance and overcome limitations encountered when using NDA alone.

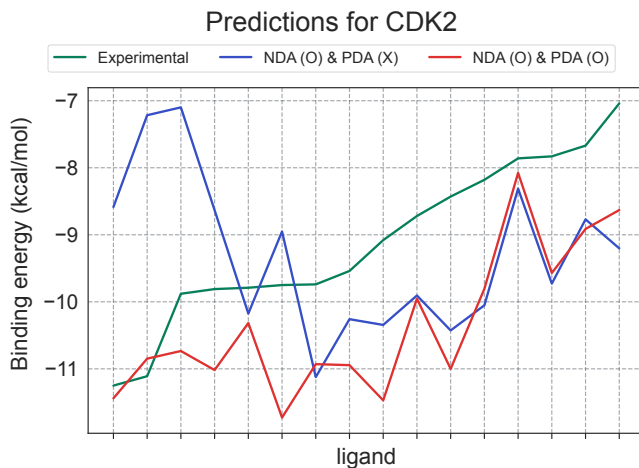


Fig. 2 A case study for a CDK2 target system for ablation study about PDA on the derivative benchmark. The CDK2 system has 16 derivatives in total, and the illustrated result is sorted based on the experimental binding energy for all derivatives. Specifically, this figure additionally illustrates the prediction results of two models: the model trained with NDA alone and the model trained with both NDA and PDA.

4 Conclusions

In this study, we present PIGNet2, a versatile deep learning-based protein-ligand interaction (PLI) prediction model that enhances its generalization ability with appropriate physics-based inductive bias and, in addition to negative data augmentation (NDA), a novel data augmentation strategy called positive data augmentation (PDA). Unlike NDA, PDA generates near-native structures treated as equivalent to crystal structures during training.

PIGNet2 incorporates both NDA and PDA, enabling accurate binding affinity prediction for near-native structures and effective discrimination between active and decoy molecules. Remarkably, the performance of PIGNet2 in the derivative benchmark is on par with the state-of-the-art model while maintaining competitive screening performance with other deep learning-based PLI prediction models designed primarily for virtual screening. This multifaceted performance solidifies the potential of PIGNet2 as a versatile deep learning-based PLI prediction model suitable for both scoring and screening tasks in drug discovery.

Despite its potential, our current data augmentation strategies have room for improvement. Currently, a generation procedure of overall structures is biased toward the scoring function of the Smina docking software. This bias results in challenges when dealing with structures that differ from those optimized by Smina. Thus, future work could explore more diverse methods for conformation generation or utilize snapshots from molecular dynamics simulation trajectories to address this limitation. Additionally, the use of NDA with the hinge loss could lead to lower predicted binding affinities for actives, as observed in the DUD-E benchmark ablation study. Future studies may consider a softer loss function for NDA or additional data augmentation strategies to enhance the overall robustness and effectiveness of PLI prediction models in the drug discovery process.

Data availability

The code and trained models are available at github: <https://github.com/ACE-KAIST/PIGNet2>. Also, data is available at <https://doi.org/10.5281/zenodo.8091220>.

Author Contributions

Conceptualization: S.M. and W.Y.K.; methodology: S.M. and J.L.; software, investigation, and formal analysis: S.M., S.-Y.H.; writing – original draft S.M.; writing – review & editing: S.M., S.-Y.H., J.L., and W.Y.K.; supervision: W.Y.K.

Conflicts of interest

There are no conflicts to declare.

Acknowledgements

This work was supported by the National Research Foundation of Korea (NRF) grant funded by the Korea government (MSIT) (RS-2023-00257479).

Notes and references

- 1 O. Guvench and A. D. MacKerell, *Current Opinion in Structural Biology*, 2009, **19**, 56–61.
- 2 A. Masoudi-Nejad, Z. Mousavian and J. H. Bozorgmehr, *In Silico Pharmacol.*, 2013, **1**, 17.
- 3 N. Hansen and W. F. van Gunsteren, *J. Chem. Theory Comput.*, 2014, **10**, 2632–2647.
- 4 J. D. Chodera, D. L. Mobley, M. R. Shirts, R. W. Dixon, K. Bronson and V. S. Pande, *Current Opinion in Structural Biology*, 2011, **21**, 150–160.
- 5 I. Muegge and Y. Hu, *ACS Med. Chem. Lett. Medicinal Chemistry Letters*, 2023, **14**, 244–250.
- 6 B. K. Shoichet, S. L. McGovern, B. Wei and J. J. Irwin, *Current opinion in chemical biology*, 2002, **6**, 439–446.
- 7 J. Fan, A. Fu and L. Zhang, *Quantitative Biology*, 2019, **7**, 83–89.
- 8 S.-Y. Huang, S. Z. Grinter and X. Zou, *Physical Chemistry Chemical Physics*, 2010, **12**, 12899–12908.
- 9 H. Li, K.-H. Sze, G. Lu and P. J. Ballester, *WIREs Comput Mol Sci Computational Molecular Science*, 2020, **11**,.
- 10 H. Öztürk, A. Özgür and E. Ozkirimli, *Bioinformatics*, 2018, **34**, 821–829.
- 11 I. Lee, J. Keum and H. Nam, *PLoS Computational Biology*, 2019, **15**, 1–21.
- 12 J. Jiménez, M. Škalič, G. Martínez-Rosell and G. D. Fabritiis, *J. Chem. Inf. Model.*, 2018, **58**, 287–296.
- 13 Y. Kwon, W.-H. Shin, J. Ko and J. Lee, *International Journal of Molecular Sciences*, 2020, **21**, 8424.
- 14 Z. Zhang, L. Chen, F. Zhong, D. Wang, J. Jiang, S. Zhang, H. Jiang, M. Zheng and X. Li, *Current Opinion in Structural Biology*, 2022, **73**, 102327.
- 15 J. Gabel, J. Desaphy and D. Rognan, *J. Chem. Inf. Model.*, 2014, **54**, 2807–2815.
- 16 C. Shen, Y. Hu, Z. Wang, X. Zhang, J. Pang, G. Wang, H. Zhong, L. Xu, D. Cao and T. Hou, *Briefings in Bioinformatics*, 2020, **22**, bbaa070.
- 17 J. Yang, C. Shen and N. Huang, *Frontiers in pharmacology*, 2020, **11**, 69.
- 18 M. Su, G. Feng, Z. Liu, Y. Li and R. Wang, *Journal of chemical information and modeling*, 2020, **60**, 1122–1136.
- 19 Z. Wang, L. Zheng, Y. Liu, Y. Qu, Y.-Q. Li, M. Zhao, Y. Mu and W. Li, *Frontiers in Chemistry*, 2021, **9**, 753002.
- 20 Y. Wang, Z. Wei and L. Xi, *BMC Bioinformatics*, 2022, **23**, 222.
- 21 O. Méndez-Lucio, M. Ahmad, E. A. del Rio-Chanona and J. K. Wegner, *Nature Machine Intelligence*, 2021, **3**, 1033–1039.
- 22 C. Shen, X. Zhang, Y. Deng, J. Gao, D. Wang, L. Xu, P. Pan, T. Hou and Y. Kang, *Journal of Medicinal Chemistry*, 2022, **65**, 10691–10706.
- 23 Z. Wang, L. Zheng, S. Wang, M. Lin, Z. Wang, A. W.-K. Kong, Y. Mu, Y. Wei and W. Li, *Briefings in Bioinformatics*, 2022, **24**, bbac520.
- 24 L. Zheng, J. Meng, K. Jiang, H. Lan, Z. Wang, M. Lin, W. Li, H. Guo, Y. Wei and Y. Mu, *Briefings in Bioinformatics*, 2022, **23**, bbac051.
- 25 C. Shen, Y. Hu, Z. Wang, X. Zhang, J. Pang, G. Wang, H. Zhong, L. Xu, D. Cao and T. Hou, *Briefings in Bioinformatics*, 2021, **22**, bbaa070.
- 26 R. Meli, A. Anighoro, M. J. Bodkin, G. M. Morris and P. C. Biggin, *Journal of Cheminformatics*, 2021, **13**, 59.
- 27 A. R. Leach, B. K. Shoichet and C. E. Peishoff, *J. Med. Chem.*, 2006, **49**, 5851–5855.
- 28 K. Huang, C. Xiao, L. M. Glass and J. Sun, *Bioinformatics*, 2020, **37**, 830–836.
- 29 T. Pahikkala, A. Airola, S. Pietila, S. Shakyawar, A. Szwajda, J. Tang and T. Aittokallio, *Briefings in Bioinformatics*, 2014, **16**, 325–337.

- 30 M. Volkov, J.-A. Turk, N. Drizard, N. Martin, B. Hoffmann, Y. Gaston-Mathé and D. Rognan, *J. Med. Chem.*, 2022, **65**, 7946–7958.
- 31 S. Moon, W. Zhung, S. Yang, J. Lim and W. Y. Kim, *Chem. Sci.*, 2022, **13**, 3661–3673.
- 32 P. G. Francoeur, T. Masuda, J. Sunseri, A. Jia, R. B. Iovanisci, I. Snyder and D. R. Koes, *J. Chem. Inf. Model.*, 2020, **60**, 4200–4215.
- 33 C. Shen, X. Hu, J. Gao, X. Zhang, H. Zhong, Z. Wang, L. Xu, Y. Kang, D. Cao and T. Hou, *J. Cheminform*, 2021, **13**, 81.
- 34 H. Li, K.-S. Leung, M.-H. Wong and P. J. Ballester, *BMC Bioinformatics Bioinformatics*, 2016, **17**, 308.
- 35 M. Su, Q. Yang, Y. Du, G. Feng, Z. Liu, Y. Li and R. Wang, *Journal of Chemical Information and Modeling*, 2018, **59**, 895–913.
- 36 M. M. Mysinger, M. Carchia, J. J. Irwin and B. K. Shoichet, *Journal of Medicinal Chemistry*, 2012, **55**, 6582–6594.
- 37 L. Wang, Y. Wu, Y. Deng, B. Kim, L. Pierce, G. Krilov, D. Lupyan, S. Robinson, M. K. Dahlgren, J. Greenwood, D. L. Romero, C. Masse, J. L. Knight, T. Steinbrecher, T. Beuming, W. Damm, E. Harder, W. Sherman, M. Brewer, R. Wester, M. Murcko, L. Frye, R. Farid, T. Lin, D. L. Mobley, W. L. Jorgensen, B. J. Berne, R. A. Friesner and R. Abel, *J. Am. Chem. Soc.*, 2015, **137**, 2695–2703.
- 38 Z. Liu, M. Su, L. Han, J. Liu, Q. Yang, Y. Li and R. Wang, *Acc. Chem. Res.*, 2017, **50**, 302–309.
- 39 H. M. Berman, *Nucleic Acids Research*, 2000, **28**, 235–242.
- 40 H. Li, K.-S. Leung, M.-H. Wong and P. J. Ballester, *Molecules*, 2015, **20**, 10947–10962.
- 41 S. Wang, J. Witek, G. A. Landrum and S. Riniker, *Journal of chemical information and modeling*, 2020, **60**, 2044–2058.
- 42 A. K. Rappé, C. J. Casewit, K. Colwell, W. A. Goddard III and W. M. Skiff, *Journal of the American chemical society*, 1992, **114**, 10024–10035.
- 43 T. A. Halgren, *Journal of computational chemistry*, 1996, **17**, 490–519.
- 44 D. R. Koes, M. P. Baumgartner and C. J. Camacho, *Journal of chemical information and modeling*, 2013, **53**, 1893–1904.
- 45 O. Trott and A. J. Olson, *Journal of computational chemistry*, 2010, **31**, 455–461.
- 46 W. Li and A. Godzik, *Bioinformatics*, 2006, **22**, 1658–1659.
- 47 L. Fu, B. Niu, Z. Zhu, S. Wu and W. Li, *Bioinformatics*, 2012, **28**, 3150–3152.
- 48 *InterBioScreen Ltd*, <http://www.ibscreen.com>.
- 49 E. W. Bell and Y. Zhang, *Journal of Cheminformatics*, 2019, **11**, 1–9.
- 50 J. Word, S. C. Lovell, J. S. Richardson and D. C. Richardson, *Journal of Molecular Biology*, 1999, **285**, 1735–1747.
- 51 P. J. Ropp, J. C. Kaminsky, S. Yablonski and J. D. Durrant, *Journal of Cheminformatics*, 2019, **11**, 1–8.
- 52 *RDKit: Open-source cheminformatics*, <http://www.rdkit.org>.
- 53 N. M. O’Boyle, M. Banck, C. A. James, C. Morley, T. Vandermeersch and G. R. Hutchison, *Journal of cheminformatics*, 2011, **3**, 1–14.
- 54 Schrödinger, LLC.
- 55 C. M. Bishop, 1994.
- 56 L. Chen, A. Cruz, S. Ramsey, C. J. Dickson, J. S. Duca, V. Hornak, D. R. Koes and T. Kurtzman, *PLOS ONE*, 2019, **14**, e0220113.
- 57 S. Kullback and R. A. Leibler, *The annals of mathematical statistics*, 1951, **22**, 79–86.
- 58 J. Sunseri and D. R. Koes, *Molecules*, 2021, **26**, 7369.
- 59 R. Quiroga and M. A. Villarreal, *PloS one*, 2016, **11**, e0155183.
- 60 H. Li, K.-S. Leung, M.-H. Wong and P. J. Ballester, *BMC bioinformatics*, 2016, **17**, 13–25.
- 61 J. Yu, Z. Li, G. Chen, X. Kong, J. Hu, D. Wang, D. Cao, Y. Li, X. Liu, G. Wang *et al.*, *ChemRxiv*, 2023, preprint, DOI: 10.26434/chemrxiv-2023-tbmtt.